Structure of the vapor–liquid interface near the critical point

J. W. Schmidt and M. R. Moldover
Thermophysics Division, National Institute of Standards and Technology, Gaithersburg, Maryland 20899

(Received 26 February 1993; accepted 16 March 1993)

We measured the thicknesses of the vapor–liquid interfaces near the critical points of carbon dioxide (CO_2), sulfur hexafluoride (SF_6), and trifluoromethane (CHF_3) using ellipsometry. The data (when scaled by the refractive index difference Δn and the correlation length ξ) are in agreement with other ellipticity data for binary and pseudobinary mixtures at low pressures. Fully constrained theories of the interface correctly predict the temperature dependence and scaling of the thickness but systematically overestimate the thickness itself by 15%–20%. The theory can be brought into agreement with experiment when an intrinsic interfacial stiffness is added to the theory. A novel feature of the present measurements is that the effects from pressure-induced window strain were measured and mitigated by using a cylindrically-symmetric pressure cell with floating seals.

I. INTRODUCTION

There are two pictures of the vapor–liquid interface near critical points and the liquid–liquid interface near consolute points that exhibit different aspects of its structure. The first one is a smooth and layered interface described by the so-called density profile theory. In this theory the density (or order parameter) varies smoothly as one proceeds from deep in the lower phase up through the interface and into the upper phase, and the interfacial thickness is approximately twice the correlation length in the two phase region ξ^-. In contrast, the second picture is a perfectly sharp interface roughened by surface modes or waves propagating on the interface. In this picture the roughness of the interface is described by capillary-wave theory in which the surface tension σ provides a restoring force. Since the interface is in a thermal bath, all possible modes contain on average $1/2\ k_BT$ of energy creating a rough interface. In capillary-wave theory the roughness provides the thickness that would be measured by experiment. Recent theories by Sengers and Van Leeuwen,[1] and by Meunier[2,3] combine both pictures of the interface and correctly predict the scaling of the thickness with the temperature-dependent correlation length and with no adjustable parameters. (Figure 1 shows a schematic representation of the composite interface.) However, these theories overestimate the thicknesses by $\sim 15\%$, including those thicknesses that we have measured using ellipsometry for five binary mixtures of low molecular weight[4,5] and three binary mixtures of high molecular weight.[6] More recently Blokhuis and Bedeaux[7] and Bonn and Wegdam[8] obtain good agreement with our measurements for binary liquid mixtures by attributing an intrinsic stiffness to the interface.

Prior to the present measurements, results near vapor–liquid critical points have been inconsistent with the Blokhuis–Bedeaux and Bonn–Wegdam theories. The only previously published ellipticity measurements[9] for the vapor–liquid interface near the critical temperature T_c were taken from carbon tetrachloride (CCl_4). They cannot be scaled as the theory predicts. Reflectivity measurements on two other vapor–liquid interfaces are also inconsistent with theory. In one system (a liquid–liquid interface)[10] the reflectivity shows the correct temperature dependence but it is 15%–20% low; in the other system (a vapor–liquid interface)[11] the reflectivity has the correct value far from the critical point but it does not have the correct temperature dependence. For a thorough discussion of the reflectivity results see Sengers *et al.*[12]

In this paper we present new ellipticity measurements near the critical points of three vapor–liquid systems, sulfur hexafluoride (SF_6), carbon dioxide (CO_2), and trifluoromethane (CHF_3). The results are similar to our previous results for binary and pseudobinary mixtures in which universal behavior was found. The principal difference between the present measurements and our earlier ones is that measurements on the binary mixtures were all made at relatively low pressures. In contrast, ellipticity measurements on pure fluids near their critical points must be made at elevated pressures where pressure-induced window strain can adversely affect the measurements. In the present measurements a novel precision thick-walled cylindrically symmetric cell with floating seals is used to mitigate strain effects.

We find that after high-pressure strain effects are properly accounted for and after the ellipticity is scaled by Δn and ξ^-, the measurements on the three fluids in this study are in agreement with the earlier low-pressure ellipticity measurements on binary mixtures. Here Δn is the refractive index difference between the upper and lower phases and ξ^- is the correlation length in the two phase region below the critical temperature. Thus both vapor–liquid interfaces and liquid–liquid interfaces yield similar results within experimental error.

II. THEORY

Intrinsic density profile theories of the interface[13,14] between near-critical fluid phases predict a universal order parameter profile $X(z/2\xi^-)$, which is a function of the spatial coordinate perpendicular to the interface, z, scaled by the bulk correlation length in the two-phase region, ξ^-.

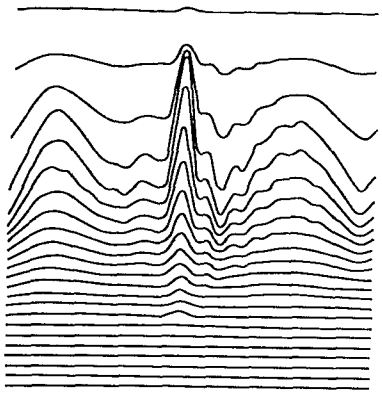

FIG. 1. A schematic representation of the interface which combines the rough (capillary-wave) and layered (mean-field) aspects of the interface. Here the line spacing represents the density which changes smoothly from the lower to the upper phase.

Fisk and Widom[15,16] have extended the theory to include fluids near nonclassical critical points, and in their theory the profile near the critical temperature is

$$X(z/2\xi^-)=\sqrt{2}\tanh(z/2\xi^-)[3-\tanh^2(z/2\xi^-)]^{-1/2}. \tag{1}$$

The function $X(z/2\xi^-)$ describes the variation of the order parameter from deep in one phase to high in the second phase. The interface described by this theory is layered and homogeneous in a direction parallel to the interface.

In contrast, capillary-wave theory describes an interface that is atomically sharp. The order-parameter profile is a step function of z/ξ^- and is roughened by thermally excited capillary waves. In this theory, the mean square wave amplitude, $\langle\zeta^2\rangle$, is comprised of all modes propagating at the interface and is given by

$$\langle\zeta^2\rangle=\frac{k_BT}{4\pi^2}\int_0^{2\pi}d\theta\int_{q_{\min}}^{q_{\max}}\frac{qdq}{g\Delta\rho+\sigma(q)q^2}, \tag{2}$$

where k_B is Boltzmann's constant, T is the absolute temperature, $\sigma(q)$ is the interfacial tension, g is the acceleration of gravity, and $\Delta\rho$ is the difference between the densities of the two phases. The integral in Eq. (2) includes all modes with wave number q between $q_{\min}$, the lowest wave number (or longest wavelength) allowed, and $q_{\max}$, the highest wave number that the interface can support. The limit $q_{\max}$ is defined as a/ξ^-, where a is a coupling constant that is expected to be of order unity. In their seminal paper on capillary wave phenomena, Buff, Lovett, and Stillinger[17] made the choice $a=\pi/4\approx0.78$. Beysens and Robert[18] used a as a fitting parameter for reflectivity data and found the value ≈0.4. While the existence of $q_{\max}$ and its variation inversely with ξ^- has been postulated for some time,[17,19] it is only recently that the magnitude of the coupling constant a has been fixed by theory and quantitative values assigned.[1–3]

The theory of Sengers and Van Leeuwen (SvL) yields the value $a=0.748$. This theory assumes a q-dependent interfacial tension, $\sigma(q)$, as implied by Eq. (2) and given explicitly by the following expression due to Kayser[19]:

$$\sigma(q)=\frac{k_BT_c}{8\pi^2}\int_0^{2\pi}d\theta\int_q^{q_{\max}}qdq\ln\left[\frac{\sigma(q)(ql^*l')^2}{2\pi k_BT_c}\right], \tag{3}$$

where $l^*=2\sqrt{\pi}/q_{\max}$, and l' is a parameter fixed by constraints. Equation (3) expresses the idea that the longer wavelength modes feel an interfacial tension that is somewhat reduced because of the presence of all modes of shorter wavelength. SvL applied three constraints to Eq. (3). First, $\sigma(q)|_{q=0}=\sigma_0$, where σ_0 is the macroscopic value of the interfacial tension; second, $\sigma(q_{\max})=\sigma_b$, where σ_b is the bare interfacial tension of intrinsic density profile theory; and third $d\sigma(q)/dq|_{q=q_{\max}}=0$. With these constraints on Eq. (3), $\sigma(q)$ and $q_{\max}$ are determined, and $\langle\zeta^2\rangle$ can be evaluated using Eq. (2).

Meunier[2,3] used a different approach for determining $q_{\max}$. He relaxed the second and third constraints on $\sigma(q)$ at $q=q_{\max}$ and chose $\sigma(q)$ to be of the simpler form

$$\sigma(q)=\sigma_0+\sigma_1q^2, \tag{4}$$

where $\sigma_1=(3/8\pi)k_BT$, and again σ_0 is the macroscopic interfacial tension. In Eq. (4), the term in q prevents the divergence of the integral in Eq. (2) without an explicit dependence on a high wave number cutoff. An effective cutoff is still needed in Meunier's theory to interpret measurements. He examined two approaches for determining the cutoff (corresponding to the two different views of the interface). In the first approach, he assumed a sharp but roughened interface and obtained the value $(\pi/2)\sqrt{\sigma_0/\sigma_1}$ for the cutoff. This value when used in Eq. (2) gives a reasonable fit to the interfacial thickness but when added to the Fisk–Widom interfacial thickness gives an ellipticity that is too large. In the second approach, Meunier equated the Fisk–Widom interfacial thickness $L_p(=2\xi/\sqrt{2\pi})$ to the following integral [an extension of Eq. (2)] over all modes with wave number higher than $q_{\max}$:

$$L_p^2=\frac{k_BT}{4\pi^2}\int_0^{2\pi}d\theta\int_{q_{\max}}^{\infty}\frac{qdq}{g\Delta\rho+\sigma_0q^2+\sigma_1q^4}. \tag{5}$$

In this case he obtained $a=0.768$. This value of a is slightly higher than that of SvL. However, the integral in Eq. (2) is slightly lower than the SvL value.

Blokhuis and Bedeaux[7] have retained the wave-vector dependent surface tension $\sigma(q)$ and $q_{\max}$ as derived by SvL but introduced a stiffness term κq^4 to the denominator of Eq. (2). This is a curvature term and expresses the idea that the interface has an inherent stiffness against bending. Meunier[2,3] has previously used this idea for the interpretation of measurements of surfactant monolayers at interfaces. As in Meunier's approach, this additional higher-order term reduces the capillary-wave amplitude and also prevents the divergence of Eq. (2) without an explicit dependence on a high-frequency cutoff. It also brings in the parameter κ which was adjusted to fit some of the experimental results. Recently Bonn and Wegdam[8] in a separate approach substituted the cutoff wave vector obtained by Meunier in an expression for the renormalized surface tension used by Sengers and Van Leeuwen to calculate the capillary wave amplitude of Eq. (2). Van Leeuwen and

Sengers[20] have shown from general arguments that the interface will be a universal function of two parameters and that the reflectivity of a vapor–liquid system will not be identical to that of a liquid mixture. Our scaled ellipticities appear to be universal and this indicates that the effect of gravity on our present measurements can be neglected.

III. TECHNIQUE: ELLIPSOMETRY

The ellipticity of an interface is defined as the reflectivity ratio r_p/r_s,

$$\rho(\theta)=r_p(\theta)/r_s(\theta)=|r_p(\theta)/r_s(\theta)|e^{i\Delta(\theta)}, \tag{6}$$

where r_p and r_s are the in-plane and out-of-plane reflectivities, respectively, and θ is the angle of incidence. A phase shift, Δ, between r_p and r_s is produced in general by a reflection from an interface as indicated above. It is often best[21] to measure the ellipticity at θ equal to the principal optical angle (Brewster's angle θ_B) in which case $\Delta=\pi/2$. $\bar{\rho}$ is then defined at this angle as the imaginary part of r_p/r_s,

$$\bar{\rho}\equiv \mathrm{Im}[\rho(\theta)]_{\theta=\theta_B}. \tag{7}$$

A. Layered interfaces

The size of $\bar{\rho}$ is a measure of the optical thickness of an interface and in the case of a layered interface such as that of the density profile theory of Fisk–Widom (FW) it is given by Drude's Equation,[22]

$$\bar{\rho}_{\mathrm{FW}}=\frac{\pi}{\lambda}\left[\frac{(n_-^2+n_+^2)^{1/2}}{(n_-^2-n_+^2)}\right]\int dz[n^2(z)-n_-^2]\times[n^2(z)-n_+^2]/n^2(z), \tag{8}$$

where n_- and n_+ are the refractive indices in the vapor and liquid phases, respectively, λ is the wavelength of the incident light, and the refractive index profile $n(z)$ is

$$n(z)\simeq\frac{n_++n_-}{2}+\frac{n_+-n_-}{2}X(z/2\xi^-). \tag{9}$$

Near the critical point,

$$n_\pm=n_c\pm\Delta_0 t^\beta/2. \tag{10}$$

Here n_c is the refractive index at the critical point, Δ_0 is an amplitude, t is the reduced temperature $(T_c-T)/T_c$, and the critical exponent β is 0.325. Near T_c, Eq. (8) reduces to

$$\bar{\rho}_{\mathrm{FW}}\approx\frac{\sqrt{2}\pi}{\lambda}\Delta n\xi^-\chi_{\mathrm{FW}}, \tag{11}$$

where the universal constant

$$\chi_{\mathrm{FW}}\approx\int dy[1-\chi^2(y)]\approx 2.28. \tag{12}$$

B. Rough interfaces

The ellipticity $\bar{\rho}_{\mathrm{cw}}$ produced by the sharp–rough interface of capillary-wave theory is given by the following expression first derived by Zielinska *et al.*[23] motivated by experimental results of Beaglehole,[21]

$$\bar{\rho}_{\mathrm{cw}}=\frac{3}{4\lambda}\left[\frac{(n_+^2-n_-^2)}{(n_+^2+n_-^2)^{1/2}}\right]\frac{k_BT}{\sigma_b}q_{\max}. \tag{13}$$

Using a result from two scale-factor universality theories,[24,25] namely, that

$$\frac{\sigma_b(\xi^-)^2}{k_BT_c}=R=0.128, \tag{14}$$

and with T near T_c we obtain

$$\bar{\rho}_{\mathrm{cw}}\approx\frac{3}{\lambda 2\sqrt{2}}\Delta n\xi^-\frac{a}{R}, \tag{15}$$

$$\approx\frac{\sqrt{2}\pi}{\lambda}\Delta n\xi^-\chi_{\mathrm{cw}}. \tag{16}$$

Note that the temperature dependence is the same as for $\bar{\rho}_{\mathrm{FW}}\propto t^{\beta-\nu}$ and is contained in the factors $\Delta n\propto t^\beta$ and $\xi^-\propto t^{-\nu}$. In Eq. (16) we have factored out quantities in parallel with Eq. (11) which leaves a group of constants that form a universal constant for capillary waves,

$$\chi_{\mathrm{cw}}=\frac{3}{4\pi}\frac{a}{R}\approx\begin{cases}1.39; & \text{SvL}\\ 1.43; & \text{Meunier}\end{cases}. \tag{17}$$

Marvin and Toigo[26] showed that the ellipticity produced by an interface that is a combination of a thick-smooth FW interface and a sharp–rough cw interface is the linear combination of the two separate ellipticities,

$$\bar{\rho}=\bar{\rho}_{\mathrm{FW}}+\bar{\rho}_{\mathrm{cw}}. \tag{18}$$

By substituting Eqs. (11) and (16) into Eq. (18) we arrive at a simple scaling result for the ellipticity of an interface,

$$\bar{\rho}\approx\frac{\sqrt{2}\pi}{\lambda}\Delta n_0\xi_0^-t^{\beta-\nu}(\chi_{\mathrm{FW}}+\chi_{\mathrm{cw}}). \tag{19}$$

Thus far the theory summarized by Eq. (19) indicates that the quantity $\bar{\rho}\lambda/\Delta n\xi^-$ is universal. Blokhuis and Bedeaux[7] have recently expanded the derivation of Eq. (13) to include effects due to the stiffness term κq^4 mentioned in the previous section. This results in a modification of Eq. (19) as follows:

$$\bar{\rho}\approx\frac{\sqrt{2}\pi}{\lambda}\Delta n\xi^-\left\{\chi_{\mathrm{FW}}+\frac{3}{4\pi}\left(\frac{k_B}{R}\frac{T_c}{\kappa}\right)^{1/2}\times\mathrm{arctgn}\left[a\left(\frac{\kappa}{Rk_BT_c}\right)^{1/2}\right]\right\}. \tag{20}$$

In further work Blokhuis and Bedeaux[27] have shown that $\kappa=\mu k_BT_c$, where μ is universal. A value of $\mu=1.1$ is consistent with all of our previous data taken from binary mixtures and the present data on pure fluids. Note that in the limit $\kappa=0$ then Eq. (19) is obtained once again. In another approach Bonn and Wegdam[8] combined the cutoff

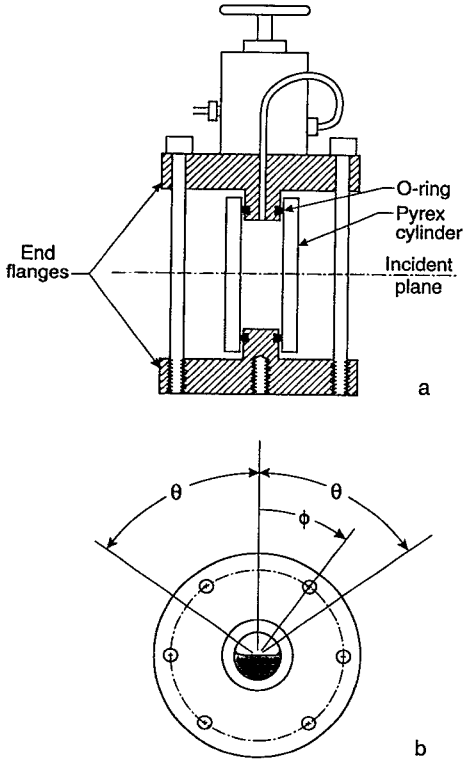

FIG. 2. (a) Horizontal section view of the pressure cell consisting of a Pyrex 7740 thick-walled cylinder, O-rings, and stainless steel end flanges. An alignment cylinder has been omitted for clarity. (b) Vertical section of the cell showing the incident and reflected angle θ, and the cell rotation angle φ.

wave vector of Meunier with the expression for the renormalized surface tension of Sengers and Van Leeuwen. They obtain a value of $\chi_{FW}+\chi_{cw}$ that is also consistent with our data.

C. Elevated pressure

The effects of window strain that were negligible in our previous work on binary mixtures at ambient pressures must be considered in the present measurements at high pressures (up to 6 MPa). The measured ellipticity, $\mathscr{R}$, due to the interface and windows acting together is

$$\mathscr{R}(\theta,\varphi)=\rho(\theta)e^{i(\Delta_1+\Delta_2)}, \tag{21}$$

where $\Delta_1=\Delta(\varphi+\theta)$ and $\Delta_2=\Delta(\varphi-\theta)$ are the additional phase shifts produced by the entrance and exit windows. φ is the azimuthal coordinate fixed to the cell itself which can be rotated about its horizontal axis of symmetry (see Fig. 2). A uniform and aligned strain is one in which either the fast or the slow axis of the stress tensor is aligned with the cell's symmetry axis. For such a strain $\Delta_1=\Delta_2$ and both windows produce phase shifts that are independent of both θ and φ. As can be seen in Eq. (21) and Fig. 3 the effect of a uniform and aligned strain is to rotate the trajectory $\rho(\theta)$ in the complex plane through an angle $\Delta_1+\Delta_2$. For this type of strain the amplitude $|\mathscr{R}|=|\rho|$ and $\bar{\rho}$ can be measured either by varying the incident angle until $|\mathscr{R}|$ is minimized, or by measuring $\Delta_1+\Delta_2$ in the straight through configuration, then adjusting the incident angle until the phase as measured by the ellipsometer is $\pi/2+(\Delta_1+\Delta_2)$ and then measuring $|\mathscr{R}|=\bar{\rho}$. Both methods are expected to be essentially equivalent and they yielded the same results within experimental error.

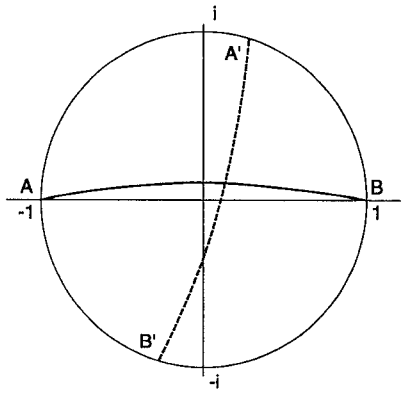

FIG. 3. The trajectory of the ellipticity in the complex plane for an interface from A (normal incidence) to B (grazing incidence) in the absence of window strain. The interfacial trajectory A'B' represents the same trajectory as AB but in the presence of window strain as described in the text. Note the distance of closest approach to the origin $\bar{\rho}$ is unchanged.

Strain in which the fast and slow axes are not aligned with the symmetry directions of the cell will affect both the measured phase and the measured amplitude. However for small amounts of nonaligned strain, $|\rho(\theta)|$ can be obtained by averaging the signal over the cell rotation angle φ at each angle of incidence. We varied the angle φ through one full rotation at each temperature and with each sample and found that $\bar{\rho}$ was unchanged. We concluded that asymmetric strain was not present in any significant amount.

The present ellipticity measurements were obtained with an automated photoelastically-modulated ellipsometer similar to one described by Beaglehole.[21] Ellipticities can be measured to within $\pm 5\%$ using this ellipsometer. In the present work, pressures as high as 6 MPa were encountered and were the main obstacle to a measurement of $\bar{\rho}$ because of the pressure-induced window strain. The next few paragraphs will describe our solution to this problem which consisted principally of maintaining cylindrical symmetry as far as possible.

IV. PRESSURE CELL DESIGN

A thick-walled cylindrically symmetric tube (Pyrex 7740), o.d. $\simeq 2.540\pm 0.003$ cm, i.d. $\simeq 1.750\pm 0.003$ cm and 5 cm long was used as the pressure vessel. The 5 cm section was selected from the best end of a 30 cm section of a precision bore tube. Inside and outside surfaces were concentric to better than 0.003 cm and the wall thickness was uniform to better than ± 0.005 cm. The length chosen was a compromise between safety and the requirement that the strain at the entrance and exit of the laser beam be as nearly uniform and aligned as possible. Locating the end

seals far from the plane of the laser beam provided a "healing" length so that strain variations were substantially reduced.

In previous experiments with cylindrical cells we had clamped stainless steel end plates with indium seals against the flat-ground glass ends and had used a torque wrench in an effort to obtain uniform axial stress. For the present measurements this design was abandoned in favor of floating end seals consisting of O-rings located on the inside of the cell. Stainless steel end flanges were used to retain the O-rings and a 0.159 cm (1/16 in.) stainless steel fill tube was welded to one of the flanges. This floating-seal design greatly reduced both the axial stress and the axial stress asymmetry. The axial stress would be zero for an infinitely long tube with the present arrangement. The remaining stress had both radial and circumferential components and their effect on the birefringence has been worked out by Nye.[28] Only the circumferential stress, σ_θ, affects the ellipticity. The resulting phase shift $\Delta_1+\Delta_2$ is

$$\Delta_1+\Delta_2=4\frac{\pi K}{\lambda}\int_a^b \sigma_\theta(r)dr, \tag{22}$$

where a and b are the inner and outer cell radii, respectively, and K is the stress-optical coefficient. The circumferential stress σ_θ for a cylindrical geometry is given by elasticity theory[29]

$$\sigma_\theta(r)=P\frac{(b^2/r^2+1)}{(b^2/a^2-1)}-Q\frac{(1+a^2/r^2)}{(1-a^2/b^2)}+R, \tag{23}$$

where P is the internal pressure, and Q is the external pressure. The constant term, $R=100$ kPa, is added to the usual equations for stress in a thick cylinder because the tube was annealed at ambient pressures. Note that Eq. (23) gives $\sigma_\theta(r)=0$ for $P=Q=100$ kPa.

The estimated bursting pressure of the cell is 25 MPa. The cell was tested to 6 MPa, the highest pressure encountered in the present measurements, with a metal plug filling most of its volume (as a safety precaution).

V. MEASUREMENTS

Each sample was distilled into the cell in an external apparatus. Then the cell was bolted to a computer-controlled precision rotational mount. Care was taken after each filling to center the cell on the rotational mount to within ± 0.004 cm. With the ellipsometer in the straight-through configuration the mount was used to rotate the cell while the window strain was measured at various angles φ. Rotating the cell caused a variation in ellipticity phase angle $\Delta_1+\Delta_2$ of approximately $\pm 2°$. This variation does not significantly affect the measurement of $\bar{\rho}$ if the ellipsometer is programmed to search for the minimum $|\mathscr{R}|$.

In Fig. 4 we have plotted the phase angle $\Delta_1+\Delta_2$ as a function of the internal pressure. The data are linear with pressure between vacuum and 6 MPa (the vapor pressure of CO_2 at 22 °C). The solid line shows the value of $\Delta_1+\Delta_2$ predicted by Eqs. (22) and (23) using the value of K for Pyrex-7740, $K=394$ (nm/cm)/(kg/mm^2) $=4.02$ nm/(m.kPa).[30] These data are consistent with Eqs. (22) and (23) and support the assertion that the strain was uniform and aligned with the symmetry axis.

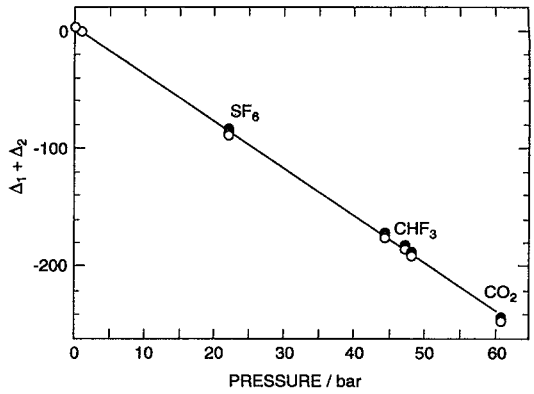

FIG. 4. Phase shift $\Delta_1+\Delta_2$ in degrees due to window strain vs internal pressure. Pressures were obtained from the vapor–liquid equilibrium pressures of Reile (Ref. 31). The solid line represents the phase shifts calculated using Eqs. (22) and (23) and Pyrex 7740 optoelastic coefficients.

All measurements were made at ambient temperature which was monitored and found to be stable over the duration (15 min) of each run to better than ± 0.05 °C. For one fluid, CHF_3, ambient temperature was adjusted toward $T_c=26$ °C. In this case the largest contribution to the errors in χ near T_c arose from the temperature uncertainty (± 0.05 °C) rather than pressure induced window strain. In the other two samples, CO_2 and SF_6, the temperature uncertainty was not as important because their respective critical points 31 and 46 °C were well above ambient (21 °C) and because $\bar{\rho}$ has a weak dependence on reduced temperature [$\bar{\rho}$ varies as $t^{\beta-\nu}\simeq t^{-0.3}$, where $t=(T_c-T)/T_c$ is the negative of the reduced temperature measured from the critical temperature].

The ellipticity data taken from SF_6 are plotted in the complex plane shown in Fig. 5(a). The plotted points appear to have been rotated clockwise with respect to the locations expected for ellipticity data from the interface itself. The rotation is exactly that expected from uniform aligned strain. The point labeled B′ on the unit circle represents a straight-through configuration in which only the windows contribute to the phase shift. The same data are represented in Fig. 5(b) rotated counterclockwise, in effect, removing the window strain. $\bar{\rho}$ is obtained from the intersection of the data with the imaginary axis in Fig. 5(b). For the figures, we have used polar/log paper in order to simultaneously display the precision of the measurements near $\bar{\rho}$ and to show point B. To analyze the data quantitatively, we have fitted a quadratic equation represented by the dashed line to the data. Thus, we obtained $\bar{\rho}$ from all the data in the vicinity of the imaginary axis, not just data taken at θ_B.

Figures 6(a) and 6(b) show data taken from the CO_2 interface treated similarly. Because this sample was at a pressure of 6 MPa the data in Fig. 6(a) appear to be rotated counterclockwise through an angle almost three times that produced by SF_6 ($\simeq 2$ MPa).

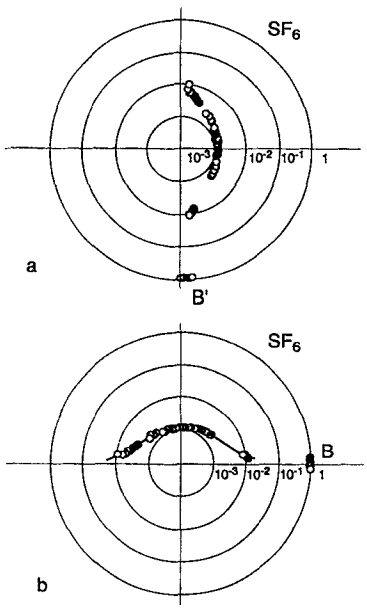

FIG. 5. (a) Ellipticity data taken from SF_6 at reduced temperature $t=0.077$ plotted in the complex plane. The data has been plotted on log/polar paper to emphasize the precision of the data near the origin and to display simultaneously the points taken in the straight-through configuration B'. (b) Same data as in (a) but with the rotation due to window strain removed.

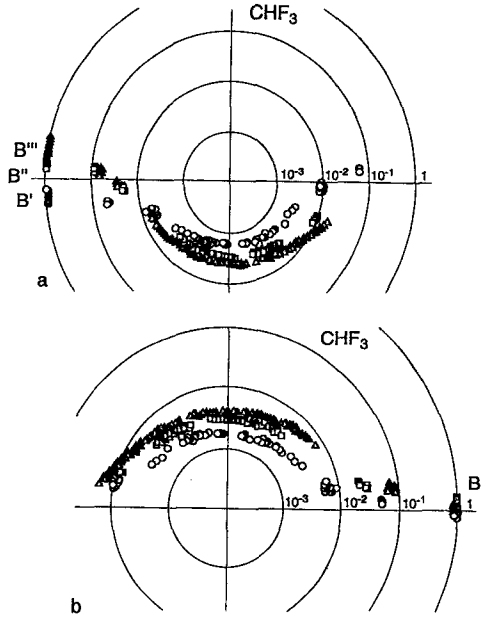

FIG. 7. (a) Ellipticity data taken from CHF_3 at three reduced temperatures $t=0.014\,9$ (circles), $t=0.003\,54$ (squares), and $t=0.000\,87$ (triangles) plotted in the complex plane as in Figs. 5(a) and 6(a). Since the pressure increases with temperature the trajectories are rotated with respect to each other. (b) Same data as in (a) but with the rotation due to window strain removed.

Figures 7(a) and 7(b) show data taken from CHF_3 at three temperatures and at several incident angles. Pressure-induced window strain which increases with temperature can be seen as an additional clockwise rotation of each data set about the origin. The phase angle $\Delta_1+\Delta_2$ due to window strain was measured at each temperature in the straight-through configuration. Figure 7(b) shows the same data as Fig. 7(a) but rotated counterclockwise by an angle equal to the phase angle measured in the straight-through configuration. As was done for SF_6 and CO_2 the data near the minimum $|\rho|$ of each trajectory of Fig. 7(b) were fitted by a quadratic equation. The intercepts of the imaginary axis $\bar{\rho}$ are recorded in Table I along with the reduced temperatures $(T_c-T)/T_c$ for each set of conditions.

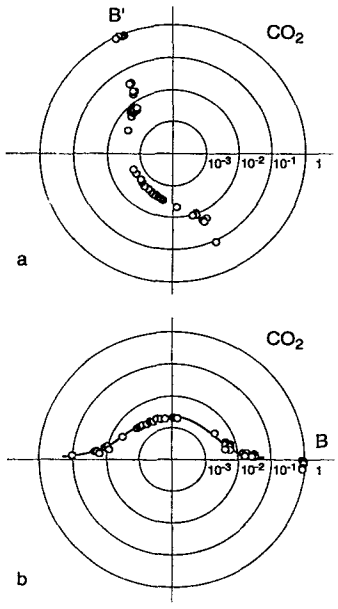

FIG. 6. (a) Ellipticity data taken from CO_2 at reduced temperature $t=0.0297$ plotted in the complex plane as in Fig. 5(a). Since the pressure ($\simeq 6$ MPa) is almost three times that of SF_6 at the same temperature the data appear to have been rotated counterclockwise through three times the angle as in Fig. 5(a). (b) Same data as in (a) but with the rotation due to window strain removed.

VI. ANALYSIS AND COMPARISONS

As indicated by Eq. (19) all measurements of $\bar{\rho}$ near T_c should yield a universal value χ when scaled by $\sqrt{2}\pi\Delta n\xi^-/\lambda$. As described in the theory section the correlation lengths were obtained from measured surface tensions and two-scale factor universality theory. The surface tensions in the case of SF_6 and CO_2 were obtained from a one-term power law equation by Do and Straub[32] and in the case of CHF_3 from Yaws *et al.*.[33] The critical temperatures listed in Table I were obtained from Do and Straub in the case of SF_6, from Levelt-Sengers and Chen[35] in the case of CO_2, and from direct observation in the case of CHF_3. Reile[31] obtained a critical temperature value for CHF_3 of 26.02 °C while Hou and Martin[34] found 25.91 °C. Our own estimates for CHF_3 put T_c at (25.86 ± 0.05) °C. Refractive index differences were obtained from Reile's correlation using our value of T_c and are given in Table I. Surface tensions were obtained from Do and Straub in the

TABLE I. Summary of measurements.

Material	T_c/°C	t	$\bar{\rho}$	Δn	σ/(mN/m)	ξ^-/nm	χ
SF_6	45.52[a]	0.077	0.001 32	0.151 8[c]	1.99[a]	0.480	2.58
CO_2	31.04[e]	0.029 7	0.001 9	0.126 1[c]	0.938[a]	0.684	3.13
CHF_3	25.86±0.05[d]	0.014 9	0.001 7	0.077 1[c]	0.340[b]	1.13	2.78
CHF_3	25.86±0.05	0.003 54	0.002 9	0.046 9[c]	0.059[b]	2.71	3.24
CHF_3	25.86±0.05	0.000 87	0.004 03	0.028 6[c]	0.010[b]	6.40	3.13

[a]Do and Straub (Ref. 32).
[b]Yaws *et al.* (Ref. 33).
[c]Reile (Ref. 31).
[d]Present estimate.
[e]Levelt-Sengers and Chen (Ref. 35).

cases of SF_6 and CO_2. For CHF_3 we used Yaws *et al.*'s correlation with our value of T_c to obtain the surface tensions.

Figure 8 shows the present measurements scaled as described above together with measurements on binary mixtures reported previously.[4–6] As can be seen the present measurements on three different pure fluids fall directly over those of the binary mixtures within the errors of the measurements. The present results differ significantly from Beaglehole's measurements[9] on the fluid CCl_4. We cannot explain the differences between CCl_4 and the present measurements.

Although Beaglehole's cell used in the CCl_4 measurement was spherically symmetric we may speculate that some of the difference was due to the possible presence of window strain in his measurements. His spherical geometry is theoretically appealing and greatly simplifies the analysis; however, it is more difficult to implement than the cylindrical geometry used in the present measurements. An additional complication in studying the critical point of CCl_4 is the high critical temperature ($T_c \simeq 245$ °C) and CCl_4 is known to decompose at high temperatures. It is possible that partial decomposition of the CCl_4 shifted its critical point and the errors in T_c could have propagated into χ. Our error bars shown in Fig. 8 could be substantially reduced by improving the thermostat.

The present measurements have resolved the discrepancy in scaling between mixtures and pure fluids. A smaller discrepancy persists between measurements and the fully constrained theory of Sengers and Van Leeuwen, and the theory of Meunier. Blokhuis and Bedeaux[7] have introduced a stiffness parameter $\kappa = \mu k_B T_c$ to obtain agreement with the measurements. The stiffness parameter provides a restoring force independent of the surface tension. Meunier[36] and Langevin and Meunier[37] had used this idea earlier in describing systems with surfactants. Subsequently, Blokhuis and Bedeaux[27] show that the stiffness parameter is universal. A value of $\mu = 1.1$ yields good agreement with the average of our measurements. Bonn and Wegdam[8] also obtain good agreement with the average of our measurements. To obtain this agreement they combine the cutoff wave vector from Meunier's theory to calculate the renormalized surface tension using Senger's and Van Leeuwen's theory.

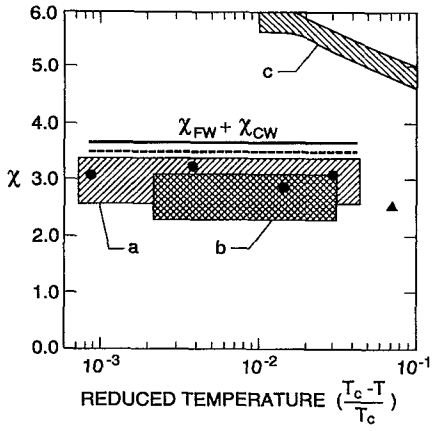

FIG. 8. The measured ellipticities, $\bar{\rho}$, of Figs. 5–7 are scaled by Δn and ξ^- and yield a system independent and temperature independent quantity χ. The lined region (a) represents measurements on simple binary mixtures (Refs. 4 and 5); the cross-hatched region (b) represents measurements on high molecular-weight binary mixtures (Ref. 6); the lined region (c) represents measurements on CCl_4 (Ref. 9); the solid line represents the theory of Sengers and Van Leeuwen; and the dashed line represents the theory of Meunier. Blokhuis and Bedeaux (Ref. 7) and Bonn and Wegdam (Ref. 8) obtain values (not shown) of χ near 3.0, the average of our measured results. Solid circles represent CHF_3; solid squares represent CO_2; solid triangles represent SF_6.

VII. SUMMARY

The thickness of the vapor–liquid interface has been measured for three fluids SF_6, CO_2, and CHF_3 using ellipsometry. The measured ellipticities from these single component systems yield values in good agreement with those from mixtures when scaled by the refractive index difference and by the correlation length. Pressure induced strain effects in cell windows which are normally a problem in these measurements were substantially removed by using cylindrical symmetry and by floating seals and by rotating the cell about the symmetry axis and averaging the results. A value for the parameter κ in the Blokhuis–Bedeaux theory of 1.1 is consistent with our data. Bonn and Wegdam obtain a value 3.02 for the universal constant χ which is close to the average of our measured values (3.0).

ACKNOWLEDGMENTS

J. W. S. acknowledges the very valuable assistance given to him by R. F. Kayser and J. V. Sengers.

[1] J. V. Sengers and J. M. J. Van Leeuwen, Phys. Rev. A **39**, 6346 (1989).
[2] J. Meunier, J. Phys. (Paris) **48**, 1819 (1987).
[3] J. Meunier, Prog. Colloid Polym. Sci. (in press); in *Liquid Matter* [Proceedings of the Liquid Matter Conference, Eur. Phys. Soc.], edited by S. Brados, 1991, p. 347.
[4] J. W. Schmidt, Phys. Rev. A **38**, 567 (1988).
[5] J. W. Schmidt, Physica A **172**, 40 (1991).
[6] D. G. Miles and J. W. Schmidt, J. Chem. Phys. **92**, 3885 (1990).
[7] E. M. Blokhuis and D. Bedeaux, Physica A **164**, 515 (1990).
[8] D. Bonn and G. H. Wegdam, J. Phys. 1 France **2**, 1755 (1992).
[9] D. Beaglehole, Phys. Rev. Lett. **58**, 1434 (1987).
[10] J. S. Huang and W. W. Webb, J. Chem. Phys. **50**, 3677 (1969).
[11] E. S. Wu and W. W. Webb, Phys. Rev. A **8**, 2065 (1973).
[12] J. V. Sengers, J. M. J. Van Leeuwen, and J. W. Schmidt, Physica A **172**, 20 (1991).
[13] J. D. van der Waals, Z. Phys. Chem. **13**, 657 (1894).
[14] J. W. Cahn and J. E. Hilliard, J. Chem. Phys. **28**, 258 (1958).
[15] S. Fisk and B. Widom, J. Chem. Phys. **50**, 3219 (1969).
[16] Review, J. S. Rowlinson and B. Widom, *Molecular Theory of Capillarity* (Oxford University, London, 1982).
[17] F. P. Buff, R. A. Lovett, and F. H. Stillinger, Phys. Rev. Lett. **15**, 621 (1965).
[18] D. Beysens and M. Robert, J. Chem. Phys. **87**, 163 (1987).
[19] R. F. Kayser, Phys. Rev. A **33**, 1948 (1986).
[20] J. V. Sengers and J. M. J. Van Leeuwen, Physica A **138**, 1 (1986).
[21] D. Beaglehole, Physica B **100**, 163 (1980).
[22] P. W. Drude, *Theory of Optics* (Longmans and Green, New York, 1902).
[23] B. J. A. Zielinska, D. Bedeaux, and J. Vlieger, Physica A **107**, 91 (1982).
[24] M. R. Moldover, Phys. Rev. A **31**, 1022 (1985).
[25] H. Chaar, M. R. Moldover, and J. W. Schmidt, J. Chem. Phys. **85**, 418 (1986).
[26] A. M. Marvin and F. Toigo, Phys. Rev. A **26**, 2927 (1982).
[27] E. M. Blokhuis, Ph.D. thesis, Rijksuniversiteit Leiden, Netherlands, 1992; E. M. Blokhuis and D. Bedeaux (private communication).
[28] J. F. Nye, *Physical Properties of Crystals* (Oxford University, London, 1964).
[29] H. M. Westergaard, *Theory of Elasticity and Plasticity* (Harvard University, Cambridge, 1952).
[30] Corning Laboratory Catalog pT9, Corning Glass Works, Corning, New York (1988).
[31] Erhard Reile, Dr. Ing. thesis, Techn. Univ. Munchen, Munchen, Federal Republic of Germany, 1981.
[32] V. T. Do and Straub, Int. J. Thermophys. **7**, 41 (1986); V. T. Do, Dr. Ing. thesis, Techn. Univ. Munchen, Munchen, Federal Republic of Germany 1982.
[33] C. L. Yaws, Haur-Chung Yang, and Xiang Pan, *Thermodynamic and Physical Property Data* (Gulf, Houston, 1992).
[34] Hou and Martin, A.I.Ch.E. J. **5**, 125 (1959).
[35] J. M. H. Levelt-Sengers and W. T. Chen, J. Chem. Phys. **56**, 595 (1972).
[36] J. Meunier, J. Phys. (Paris) Lett. **46**, L-1005.35 (1985).
[37] D. Langevin and J. Meunier, *Photon Correlation Spectroscopy and Velocimetry*, edited by H. Z. Cummins and E. R. Pike (Plenum, New York, 1977).